Evolving enhanced topologies for the synchronization of dynamical complex networks

Thomas E. Gorochowski
Bristol Centre for Complexity Sciences, Department of Engineering Mathematics, University of Bristol, Bristol BS8 1TR, United Kingdom

Mario di Bernardo
Department of Engineering Mathematics, University of Bristol, Bristol BS8 1TR, United Kingdom
and Department of Systems and Computer Science, University of Naples Federico II, Via Claudio 21, 80125 Napoli, Italy

Claire S. Grierson
School of Biological Sciences, University of Bristol, Bristol BS8 1UG, United Kingdom
(Received 19 December 2009; revised manuscript received 22 March 2010; published 21 May 2010)

Enhancing the synchronization of dynamical networks is of great interest to those designing and analyzing many man-made and natural systems. In this work, we investigate how network topology can be evolved to improve this property through the rewiring of edges. A computational tool called NETEVO performs this task using a simulated annealing metaheuristic. In contrast to other work which considers topological attributes when assessing current performance, we instead take a dynamical approach using simulated output from the system to direct the evolution of the network. Resultant topologies are analyzed using standard network measures, *B* matrices, and motif distributions. These uncover the convergence of many similar features for all our networks, highlighting also significant differences between those evolved using topological rather than dynamical performance measures.

DOI: 10.1103/PhysRevE.81.056212 PACS number(s): 05.45.Xt

I. INTRODUCTION

Synchronization plays a critical role orchestrating the coordination of many natural and man-made processes [1]. These span areas from circadian rhythms in biology [2,3] to communications via chaotic channels in engineering [4]. With applications across many types of complex system, the phenomenon has seen much attention over recent years with attempts made to understand *stability criteria* [5] and find *optimal network topologies* [6].

Understanding how and when synchronization occurs is of great importance when analyzing natural processes and building synchronous systems of our own. This involves stability analysis of the invariant manifold associated with the synchronous state in phase space. Many different types of dynamical system have been studied, showing a wide range of behaviors such as *clustering* [7,8], *phase synchronization* [9], and *desynchronizing bifurcations* [10].

In general, synchronization is studied by considering a network of *N*-coupled *m*-dimensional systems described by

$$\dot{\mathbf{x}}_i = \mathbf{F}(\mathbf{x}_i) - \sigma \sum_{j=1}^{N} \mathcal{L}_{ij} \mathbf{H} \mathbf{x}_j, \quad i = 1,2,\ldots,N, \tag{1}$$

where $\mathbf{x}_i \in \mathbb{R}^m$ is the state vector for the ith node, $\mathbf{F}:\mathbb{R}^m \rightarrow \mathbb{R}^m$ defines the internal node dynamics, $\sigma \in \mathbb{R}$ is the coupling strength between connected nodes, $\mathcal{L}=(\mathcal{L}_{ij})$ is the network Laplacian, and $\mathbf{H} \in \mathbb{R}^{m \times m}$ is a matrix specifying the inner coupling between states of two interacting nodes.

The network is then said to be *completely* or *asymptotically synchronized* if $\lim_{t\rightarrow\infty}\|\mathbf{x}_i - \mathbf{x}_j\| = 0$, while *bounded synchronization* is achieved if $\lim_{t\rightarrow\infty}\|\mathbf{x}_i - \mathbf{x}_j\| \leq \varepsilon$ for some sufficiently small $\varepsilon > 0$. The aim of this paper is to investigate how synchronization of a dynamical network can be *enhanced* in some way through optimization of the underlying topology. Generally, enhanced synchronization has been linked to the *network synchronizability*, i.e., the range of coupling strengths over which the synchronization manifold $\mathbf{x}_1 = \mathbf{x}_2 = \cdots = \mathbf{x}_N$ is locally stable. Pecora and Carroll showed how a *master stability function* (MSF) can be formulated for coupled dynamical networks and linked synchronization to the eigenvalues of the network Laplacian $\lambda_1, \lambda_2, \ldots, \lambda_N$ [5]. Specifically, if λ_N/λ_2, known as the *eigenratio* (ER), is minimized, the network will see a locally stable synchronization manifold for the largest range of coupling strengths.

There has been a lot of interest in recent years in optimizing networks using this purely *topological measure* [6,11,12]. However, this approach only considers a single characteristic of synchronization and may not be the best choice when specific constraints exist on node and edge dynamics or the network structure itself. For example, it may be that one requires enhanced synchronization to only occur near a specified coupling strength or for the largest possible coupling strength supported by a fixed number of nodes and edges. At this point, the general nature of the eigenratio limits its application. Instead, we propose an approach that uses a *dynamical measure* based on the *order parameter* introduced by Yook and Meyer-Ortmanns [13], calculated from simulated dynamics during network optimization. This has the advantage that any required dynamical features can be more easily described, but comes at the cost of computationally expensive numerical simulation.

In this work, we propose a general tool for evolving networks such that some performance measures are enhanced. We apply this tool to investigating optimal network topologies for synchronization and analyze the features of the resulting networks. We also relate our findings to results based on optimizing the Laplacian eigenratio [6,11,12] by using dynamical simulations of the node dynamics during evolution.

This paper has been organized in the following way. Section II provides a background overview on previous work which has attempted to enhance network synchronization. Next, Secs. III–V present our dynamical approach to this problem, the computational framework used to carry this out, and analysis of the resultant evolved topologies we generate. This highlights some interesting characteristics which are related to competing factors during the evolutionary process. Finally, Sec. VI considers the problem of systems that do not contain a shared synchronized trajectory due to parameter mismatch in oscillator dynamics. Using a dynamical performance measure based on minimizing the bound on distances between trajectories, we show topology has the greatest effect on systems with small deviations in node dynamics. We also analyze features of the resultant topologies and link this to the findings of the previous sections.

II. ENHANCING SYNCHRONIZATION: BACKGROUND

One of the first computational approaches to enhancing synchronization was presented by Donetti *et al.* in [6]. Topologies were analyzed that emerged when attempting to evolve networks that optimized the network eigenratio, a common measure of synchronizability. They used networks of a fixed size and average degree, with only edge rewiring permitted. As the eigenratio is calculated directly from the eigenvalues of the network Laplacian, there was no need for consideration of system-level dynamics through simulation. Results showed that optimized topologies converged to homogeneous networks with short path lengths, little clustering, and narrow degree and betweenness distributions. Such networks were termed "entangled" and similarities were also seen with *cage graphs* for some network sizes [14]. This work has since been extended with improvements that incorporate additional graph theoretic knowledge. Rad *et al.* [11] showed how convergence to a near-optimal solution could be increased ($\approx 2N$ steps) compared to random rewiring techniques. This was achieved by adding edges based on the eigenvector of the second-smallest eigenvalue of the network Laplacian and removing edges based on the current node degree. Attempts have also been made to translate the problem of network Laplacian eigenvalue optimization into a form amenable to *convex* techniques. Boyd [12] showed that by having the option to choose edge weights of an undirected graph, many standard problems related to synchronization, such as *fastest mixing* and *minimum total effective resistance*, could be described as the minimization of a convex function. The major benefit of this approach is that although it may not lead to a pure analytical solution, efficient numerical methods exist to find the *optimal* configuration.

Evolution of networks has also seen interest when attempting to make sense of features exhibited by natural systems [15–17]. Much of this has revolved around the search for genetic or neural networks that perform specific functions, the *robustness* of these systems, and the formation of *modular* hierarchies. Computational evolution has been used with models of biochemical components to find networks that perform as bistable switches and oscillators [18–20]. These types of studies have helped gain an understanding of the role differing component dynamics have in such networks and also the influence of external factors. For example, Kaneko [21] showed how certain levels of noise were necessary during evolution of transcriptional network models to generate systems robust to mutations in the network structure.

In relation to modularity, the idea of *network motifs* [22,23] has become popular. With complex systems being composed of huge numbers of interacting parts, analyzing or building such systems with specified behaviors becomes a daunting task; unless there are ways of breaking the problem into smaller, compossible parts. Milo *et al.* illustrated that natural evolution may have tackled the problem in this way using modularity and specifically network motifs [24]. These are defined as small subgraphs expressed more often than would be expected by random chance [22]. They have been shown to relate to specific information processing capabilities [25–27] and also studied in regards to their synchronization properties [28].

III. DYNAMICAL APPROACH

In this section, a computational tool called NETEVO will be used to investigate networks that have been optimized for both topological and dynamical measures in an attempt to classify and link topological structures with dynamical features of the synchronization exhibited. We impose the additional constraints that all networks are unweighted and undirected, leading to a Laplacian matrix that is symmetric with zero row sums and consider networks of 100 nodes with an average degree of $\langle k \rangle = 4$. Changes to the topology can be made through the rewiring of links, however, the number of nodes and edges remains fixed in an attempt to reduce the influence of differing available resources on final topologies.

A. NETEVO framework

To carry out the analysis, we developed NETEVO [29], an open-source computational framework designed to facilitate the investigation of evolutionary processes of dynamical complex networks and bring together simulation, evolution, and analysis in a coherent way. To do this, we present the idea of a *supervisor* who is solely responsible for making decisions on how network structure and model parameters should be altered to help meet a performance measure Q. To aid in this task, the supervisor is privy to all system states and can, if necessary, be restricted by user constraints. The principle of a supervised network is illustrated in Fig. 1. As this can in many ways be viewed as a standard optimization method with an unknown relationship between performance and configuration, a combinatorial search is required. To carry this out, the framework uses a *simulated annealing* metaheuristic [30] to help find near-optimal states.

To allow for wide spread use, the framework has been designed in a modular fashion allowing for users to easily define their own specific node or edge dynamics, performance measures, and methods for evolution. At present, only dynamics in the form of ordinary differential equations are supported, however, we hope to broaden this to discrete and stochastic processes.

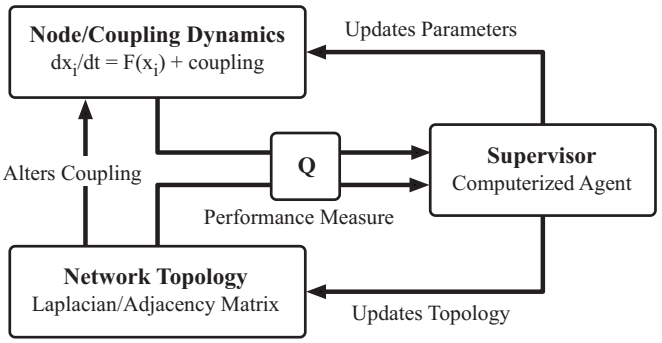

FIG. 1. Flow diagram of a supervised network.

Extensive use has been made of several well-established open-source scientific libraries, maximizing code reuse and quality. This includes *igraph* [31] for storage and analysis of network topologies and the *GNU Scientific Library* [32] for numerical integration and spectral methods. With speed and portability being a major consideration for large scale simulation, the framework has been coded purely in C. This has the added benefit of possible future access to high performance technologies such as MPI, OPENMP, and OPENCL, while allowing for easy embedding into prototyping and scripting languages such as PYTHON and RUBY. For further information regarding the framework, see http://www.netevo.org. In what follows, we use NETEVO to explore the open problem of evaluating the evolution of dynamical networks to enhance synchronization.

B. Network optimization

Optimization of the network topology was performed using NETEVO and a similar approach to that in [6]. The simulated annealing-based supervisor was chosen with a standard rewiring mutation that was performed after each trial to generate a new candidate configuration. The number of edges rewired between trials was selected from an exponentially distributed random variable with mean $\bar{x}=1$. The initial temperature T was estimated by $4q_{\max}$, where $q_{\max}$ was the maximum difference in the performance measure Q for 100 pretrial runs. The temperature then remained fixed for each trial at a given step and reduced by 10% once the step was complete. There was a maximum of 5000 trials per step or 500 consecutive accepting trials. A new state was accepted if the configuration had an improved Q or otherwise with probability $e^{-dQ/T}$, where dQ is the change in performance measure and T is the current temperature. A final configuration was chosen after five consecutive temperature reductions with no change in topology. Halting was ensured by imposing a maximum of 500 000 trials or a minimum temperature of 10^{-7}, whichever was reached first.

To ensure a range of features was seen in our system and to compare our results to those in the existing literature, we chose a chaotic Rössler regime as a testbed example where $\mathbf{x}_i=(p_i,q_i,r_i)$, selecting diffusive coupling via p and r variables so that the network is described by Eq. (1) with

$$\mathbf{F}(\mathbf{x}_i)=\begin{cases}-q_i-r_i\\ p_i+0.165q_i\\ 0.2+(p_i-10)r_i,\end{cases} \tag{2}$$

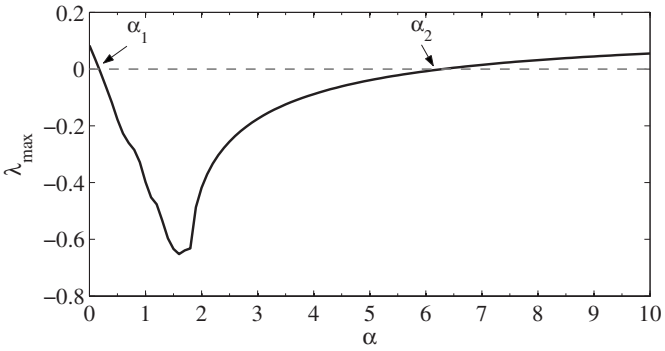

FIG. 2. Master stability function for the chosen Rössler system with $\alpha_1\approx 0.2$ and $\alpha_2\approx 6.1$. A method presented in [34] was used to calculate the maximal Lyapunov exponent $\lambda_{\max}$.

$$\mathbf{H}=\begin{pmatrix}1&0&0\\0&0&0\\0&0&1\end{pmatrix}. \tag{3}$$

This choice of coupling leads to a master stability function that is only stable within a bounded region (α_1,α_2). Figure 2 shows the master stability function (MSF) for this particular system. This MSF is of class Γ_2 according to classification reported in the literature [33], giving a locally stable range of $\alpha\in(0.2,6.1)$. Therefore, the network will be synchronized if $\sigma\lambda_2>\alpha_1$ and $\sigma\lambda_N<\alpha_2$. This is particularly well suited for our study since this limited range of stability will allow us to evaluate the influence of network topology on tuning overall features such that the stability conditions are satisfied.

To simulate system dynamics, the ODE solver module was configured to use the embedded Runge-Kutta-Fehlberg (4, 5) numerical method with an adaptive step size and absolute and relative errors of 10^{-5}. Simulations lasted for 150 time units and consisted of ten separate runs from different initial conditions to give averaged performance measure values. This helped to minimize any effects due to finite simulation times. Initial conditions were chosen uniformly at random on the interval [0, 20] for all states.

We selected the eigenratio and order-parameter performance measures to optimize our networks. With the eigenratio acting as a baseline due to its prevalence in the literature, the order parameter was chosen to give a purely dynamical view of the system and establish the benefit this may provide. The order parameter $\mu(t)\in[0,1]$ was calculated using

$$\mu(t)=\frac{1}{N(N-1)}\sum_{i=1}^{N}\sum_{j=1}^{N}\Theta[\delta-d_{ij}(t)], \tag{4}$$

where N is the number of nodes, Θ is the Heaviside function, δ is a threshold distance around the synchronization manifold, and $d_{ij}(t)$ is the standard Euclidean norm distance between trajectories for nodes i and j at time t. This returns the fraction of pairs of nodes that are synchronized. Due to optimization in our system leading to the minimization of a given function, the final performance measure is given by $Q_{OP}=1-\mu(t_\infty)$, where t_∞ is defined as the network *settling time*, i.e., the time instant such that for $t>t_\infty$ all trajectories

TABLE I. Statistical analysis of the initial topologies.

Topology	Diameter	Clustering	Eigenratio
Lattice	25	0.50	365.9
Random	7	0.03	31.3
Scale-free	6	0.06	65.3
Small-world	8	0.17	41.7

have converged within the region defined by the chosen δ. In what follows, t_∞ is estimated heuristically via simulations.

The global coupling strength σ was chosen to remain fixed throughout each optimization process and then varied to compute the synchronization response of the evolved topology. To avoid confusion, we will refer to $\hat{\sigma}$ as the value of the coupling used during each optimization. We will use σ to denote the value of the coupling used in post-processing simulations to evaluate the synchronizability and features of the evolved topologies.

To reduce the influence of initial topologies on final configurations, several types of initial networks were used including random, lattice, scale-free, and small world [35]. Unless otherwise stated, all evolved networks converged to a similar final state. The main statistical properties of the initial topologies are reported in Table I.

To analyze the synchronization characteristics of a given network topology, we generated what is termed a *synchronization response* graph. This uses simulated dynamics of a network topology for a range of different coupling strengths σ and plots after a sufficient period of time the fraction of nodes in a synchronous regime, as defined in Eq. (4).

In subsequent sections, we conduct the following numerical experiments:

(i) First, we use NETEVO to evolve networks by considering as a *static* cost function the possible Laplacian eigenratio which, according to the MSF analysis, is associated with the best synchronizability properties, i.e., the widest range of values of σ that ensure the network achieves asymptotic synchronization.

(ii) Then, having fixed $\hat{\sigma}$ to different values in the range $\hat{\sigma} \in [0.1, 0.7]$, we evolve networks by taking as a *dynamic* cost function the order parameter defined in Eq. (4). This is computed by simulating the entire network dynamics.

Particular attention will be given to the limit case $\hat{\sigma}=0.7$ which exhibits some interesting properties as further explained in Sec. IV.

C. Initial and eigenratio-evolved networks

We start with the case where the Laplacian eigenratio is used as a performance measure during the optimization procedure. The main results are shown in Fig. 3(a) where average synchronization response curves are plotted for both initial and evolved topologies.

It is evident that every initial network had a poor response across all coupling strengths. Only the random and small-world topologies saw any measurable synchronization $\approx 10\%$ for a limited range of coupling strengths.

In contrast, Fig. 3(a) shows how eigenratio evolved networks displayed full synchronization over a wide range of coupling strengths, between $\sigma=0.3$ and 0.6. Moreover, the analytically estimated synchronized range of (0.196, 0.789), calculated using $\langle \lambda_N \rangle = 7.73$ and $\langle \lambda_2 \rangle = 1.02$, coincides with the response seen from numerical simulations. Transition to and from a desynchronized state takes a sigmoid-like form over a range $\Delta\sigma \approx 0.15$. An example of an eigenratio-evolved network can be seen in Fig. 4(a). The difficulty in visually isolating any localized features is not merely an artifact of the embedding, but also due to the topological properties of the network. Structurally, the networks generated have similar *entangled* features as described in [6]; a small diameter and very little clustering due to an average girth (smallest loop within the network) equal to 3.75. They also exhibit a narrow degree distribution centered around $\langle k \rangle = 4$ (shown in Fig. 5) giving a very homogeneous appearance for many network measures, while still maintaining short path lengths unlike a standard lattice. The topological features of the various evolved networks are summarized in Table II. In the rest of this paper, we will refer to these as eigenratio evolved networks.

D. Order-parameter-evolved networks

We now turn our attention to the case where the cost function is chosen to be the order parameter itself computed at every step of the optimization procedure by directly simulating the entire network dynamics. The synchronization response for each network is shown in Fig. 3(b) with a bell-shaped curve exhibited by all networks. In many cases, however, this was not centered about the fixed $\hat{\sigma}$ selected for optimization. Instead, there appeared to be a lower bound $\sigma \approx 0.25$ under which no response was found. The location of this bound is controlled by λ_2, dictating when the smaller eigenvalues enter the stable region of the master stability function [36].

In terms of specific responses, networks evolved for $\hat{\sigma} \in [0.1, 0.4]$ see a steady increase in the total synchronization achieved, centered around $\sigma=0.45$ and ranging from 8% to 90%. Following this, both $\hat{\sigma}=0.5$ and 0.6 networks have close to full synchronization peaking near their optimized coupling strengths. When comparing structural properties, Table II shows that as networks are evolved for increasing $\hat{\sigma} \in [0.1, 0.5]$ they display a reducing diameter and eigenratio. In addition, the diameter and eigenratio properties reduce in variance, while clustering maintains a similar variance throughout.

Visualizations of the networks evolved using this measure for fixed coupling strengths are shown in Figs. 4(b)–4(f). The majority of these possess many similarities to the previous eigenratio-evolved networks and display a convergence toward reduced heterogeneity in terms of node degree; also confirmed by the average degree distribution plotted in Fig. 5(b).

The $\hat{\sigma}=0.6$ network shows some interesting differences. Topologically, the diameter and clustering increase, while the eigenratio is still reduced in comparison to previous order-parameter-optimized networks. The response, however, dis-

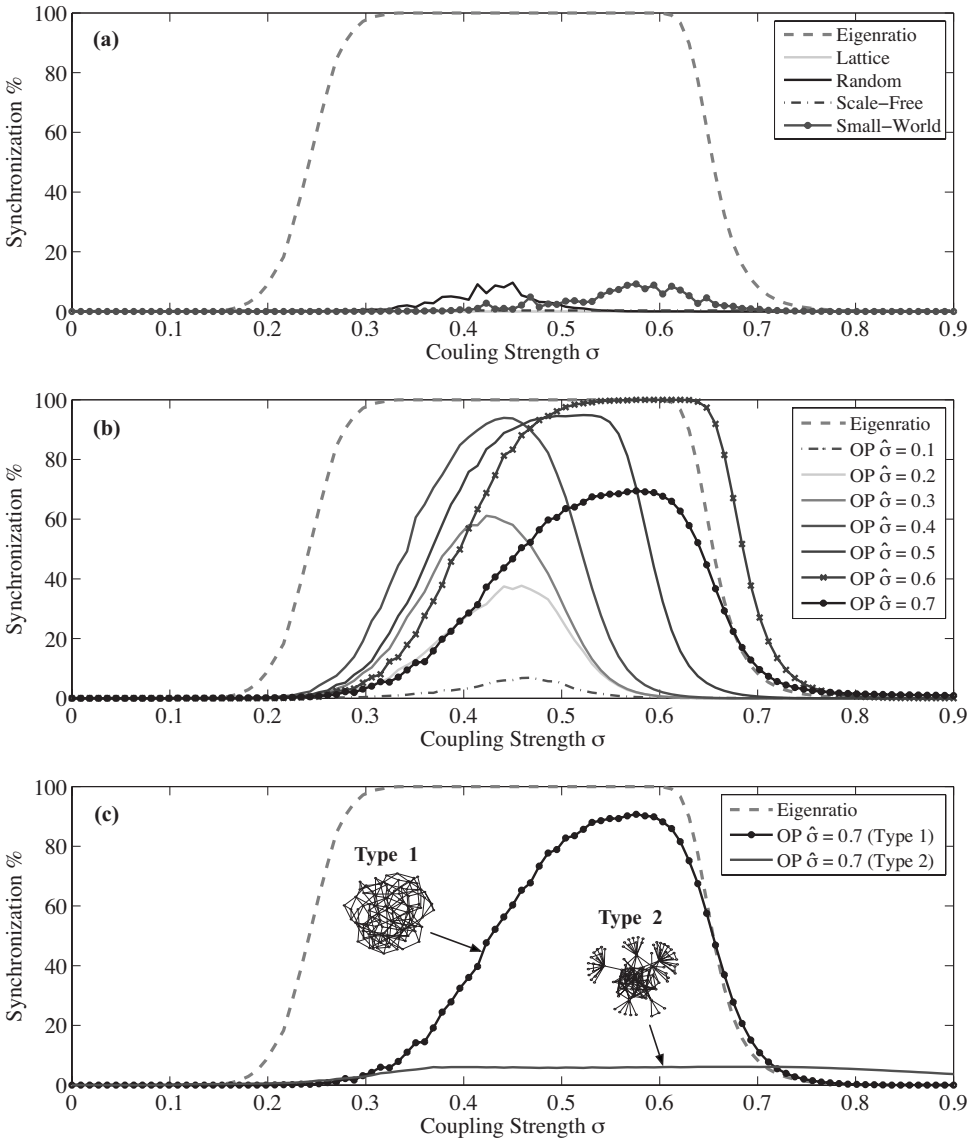

FIG. 3. Synchronization response curves showing the percentage of synchronization as the simulation coupling strength σ is varied. (a) shows averages for the initial topologies and eigenratio-evolved networks. (b) displays average results for order-parameter-evolved networks with fixed coupling strengths $\hat{\sigma} \in [0.1, 0.7]$. (c) shows average results for a break down of each type of topology found at bistable point where $\hat{\sigma}=0.7$.

plays the most surprising result improving the *upper bound* of σ for which full synchronization is seen [see Fig. 3(b)]. This is possibly due to a reduced $\langle \lambda_N \rangle = 7.47$, leading to a higher threshold $\sigma_{\max}=0.817$ at which desynchronization occurs. This is an improvement of 0.03 (6%) over the eigenratio-evolved networks. It is unclear the exact mechanism by which λ_N is reduced, however, the order-parameter-optimized network does exhibit a narrow degree distribution with over 80% of nodes having degree 4 in comparison to around 55% for eigenratio evolved networks. With

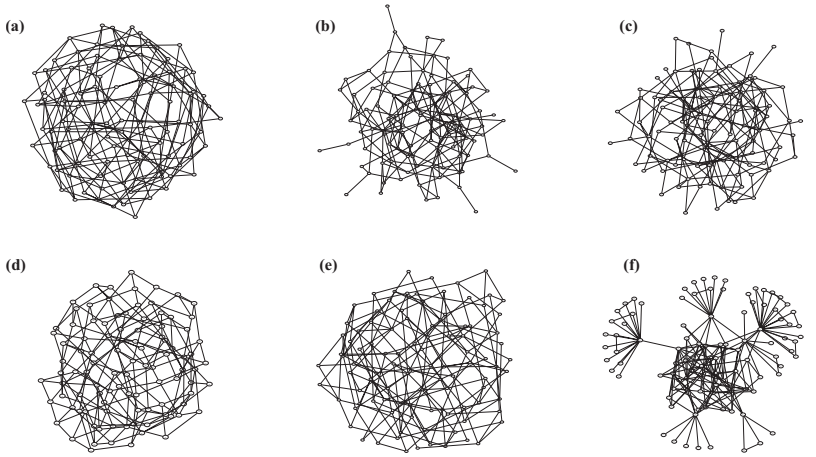

FIG. 4. Final topologies for a selection of performance measures: (a) eigenratio, (b) order parameter $\hat{\sigma}=0.1$, (c) 0.3, (d) 0.6, (e) 0.7 (type 1), (f) 0.7 (type 2). Visualization was performed using a forced based layout to help minimize edge crossing.

TABLE II. Statistical analysis of the evolved topologies.

Evolved topology	Diameter		Clustering		Eigenratio	
Performance measure	Average	Std dev	Average	Std dev	Average	Std dev
Eigenratio	5.25	0.4443	0.0029	0.0036	7.57	0.11
Order parameter $\hat{\sigma}=0.1$	7.50	0.8272	0.0581	0.0163	45.35	29.33
Order parameter $\hat{\sigma}=0.2$	6.95	0.6863	0.0219	0.0092	29.94	12.92
Order parameter $\hat{\sigma}=0.3$	6.05	0.3940	0.0271	0.0111	19.48	2.92
Order parameter $\hat{\sigma}=0.4$	6.05	0.2236	0.0177	0.0102	15.28	1.77
Order parameter $\hat{\sigma}=0.5$	6.00	0.0000	0.0287	0.0145	14.50	3.63
Order parameter $\hat{\sigma}=0.6$	6.20	0.4104	0.0917	0.0175	12.53	0.58
Order parameter $\hat{\sigma}=0.7$ (type 1)	6.33	0.4880	0.0748	0.0313	15.08	1.87
Order parameter $\hat{\sigma}=0.7$ (type 2)	6.20	0.4472	0.1155	0.0085	291.95	80.17

$\lambda_N \in [k_{\max}, 2k_{\max}]$ and $\langle k \rangle = 4$ being the lower bound for $k_{\max}$ due to the number of nodes and edges being fixed, increased homogeneity will push the network nearer to this bound. This conclusion is supported by findings in [37]. Networks evolved using $\hat{\sigma}=0.7$ show a remarkably different behavior that will be discussed in the next section.

IV. BISTABILITY AND A TOPOLOGICAL BIFURCATION

So far, evolution of networks has resulted in a single type of final topology. However, upon reaching $\hat{\sigma}=0.7$, the onset of *bistability* is detected. Specifically, out of the 20 separate evolutions that were run, 15 resulted in structures similar to those seen previously for lower values of $\hat{\sigma}$ while five led to structures with highly different topological features. We term the former *type 1* and the latter *type 2* and examples are shown in Figs. 4(e) and 4(f), respectively. Although type 1 networks maintain similar statistical properties to order-parameter-evolved networks at lower coupling strengths, there was a small increase in the diameter and eigenratio, with a reduction in clustering when compared to networks optimized for $\hat{\sigma}=0.6$. The synchronization response again took the form of a bell-shaped curve centered around $\sigma=0.58$ with a maximum response $\approx 90\%$ [see Fig. 3(c)].

Type 2 networks showed dramatically different topological statistics, maintaining a low diameter while having a large increase in clustering and eigenratio. These networks also exhibited a number of other characteristics. Figure 4(f) shows their unusual structure of separated hubs made up of triangles and single degree nodes, linked via a heavily interconnected central region. Surprisingly, there was also conservation in quantitative properties of these features, with all type 2 networks containing a similar number of hubs (5–6) and size of central region ($\approx$40 nodes).

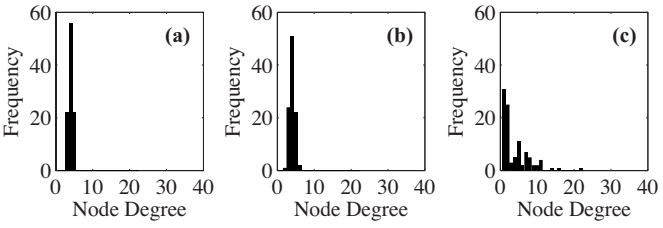

FIG. 5. Degree distributions for a selection of the evolved networks. (a) Eigenratio. (b) Order parameter $\hat{\sigma}=0.7$ (type 1). (c) Order parameter $\hat{\sigma}=0.7$ (type 2).

Another interesting aspect of the resultant topologies was their synchronization response. Unlike previous networks, only limited partial synchronization $\approx 10\%$ was exhibited, but over a much larger range of coupling strengths ($\Delta\sigma \approx 0.8$) and for strengths where no previous synchronization had been seen before ($\sigma > 0.8$). The large value of the eigenratio reported in Table II explains the poor synchronization performance being observed.

Note that the bistable region is located at the edge of the synchronizability range of the network of interest. At this point, $\sigma\lambda_N$ becomes larger than the upper limit α_2 in Fig. 2. As the coupling strength is increased further, larger numbers of eigenvalues shift into the unstable region so that type 1 networks cannot be obtained any longer. As shown in Fig. 6(c), the internal structure of the eigenspectrum of type 2 networks is such that these networks manage to maintain a larger subset of eigenvalues in the stable region of the master stability function. Thus, for larger values of $\hat{\sigma}$, we expect all optimization procedures to converge toward type 2 rather than type 1 networks.

In an attempt to estimate the extent of the bistable region, additional network evolutions were performed using $\hat{\sigma}=0.8$ and 0.9. Out of the 16 runs completed for each fixed coupling strength, all resulted in type 2 topologies with the same characteristics. This gave a maximum possible region of $0.6 < \hat{\sigma} < 0.8$ for which both types of topologies may coexist.

A. Network differentiation

To understand the deciding factors for the differentiation between type 1 and 2 networks, we investigated the changes made during the evolutionary process. We searched for points that determined network fate and analyzed the features that these possessed. Figure 7 illustrates the two possible outcomes for our networks, with some intermediate configurations during the evolutionary process. Significant differences can be seen between these, with type 1 networks maintaining node degrees above 1 and type 2 networks in-

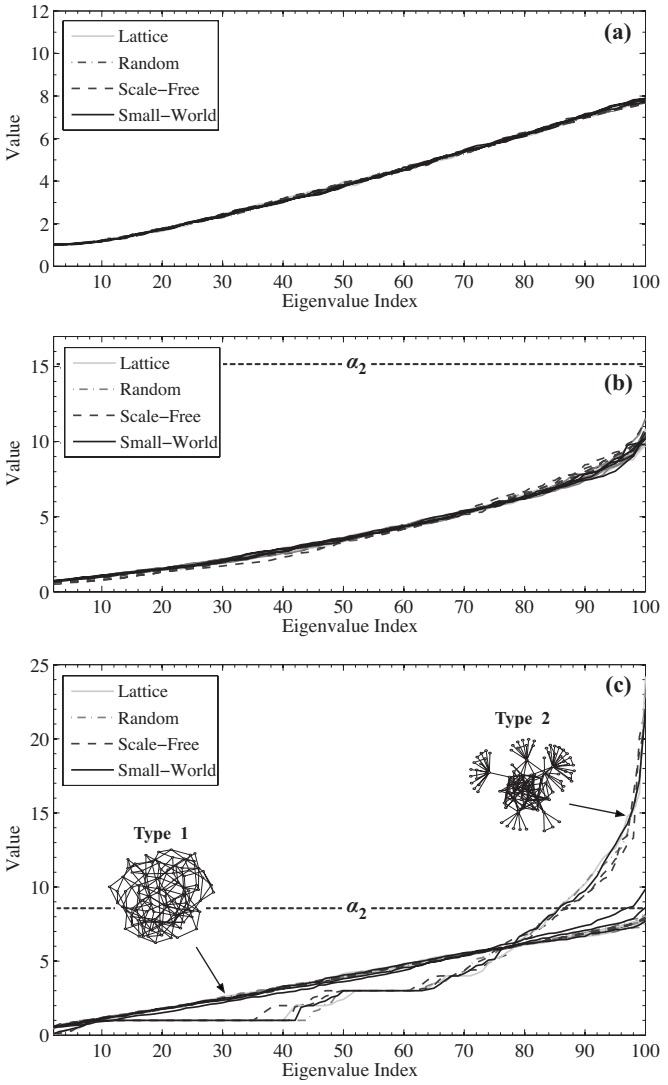

FIG. 6. Eigenspectra for (a) eigenratio, (b) order parameter $\hat{\sigma}=0.4$, and (c) order parameter $\hat{\sigma}=0.7$ evolved networks. Each line represents a single final topology for different initial conditions.

creasing the number of single degree nodes at selected hubs within in the network. Figure 8 shows how the number of single degree nodes changes over time for both types of network. There is an initial period of random variation around approximately seven nodes for both types, but then by iteration 30 000 full differentiations into each type has occurred,

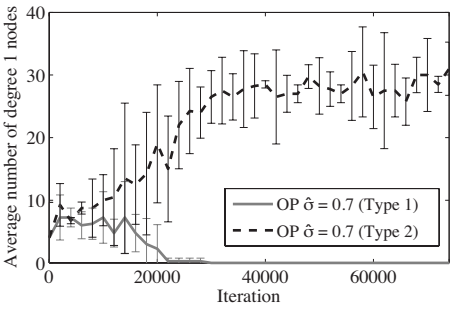

FIG. 8. Average number of single degree nodes and standard deviation during the evolution of type 1 and 2 topologies.

with type 1 networks containing none and type 2 an average of 30 single-degree nodes. This diagram also demonstrates a significant separation between each of the types, with what appears to be a threshold number of single degree nodes ≈ 16, which once reached causes only type 2 networks to arise.

A possible explanation for the single-degree nodes threshold during differentiation is a culmination of two factors: the simulated annealing process and the number of seeding nodes that have a degree of 1. Temperature forms an important part of the simulated annealing process. Initially, a high temperature is used, to allow for the system to easily move around configuration space, even if this involves areas of lower fitness. This allows for the escape from any local minima. As the process continues, the temperature is slowly reduced, making it more difficult to escape any current minima. The bistability we see could therefore be the result of the initial randomizing steps at high temperature, placing the system in a configuration between the two types of final state and as the temperature is reduced, the configuration falls either side depending on its exact location. Once the temperature is sufficiently low, it may then become impossible to traverse the suboptimal peak between the two final states. If this is the case, then the threshold would act as a determinant as to which side the configuration will fall.

The rapid speed at which type 2 topologies converge to a similar increased number of single degree nodes and the high variability in this level are also shown in Fig. 8. This feature can be explained by considering the process of hub growth. Each hub connects to a number of single degree nodes and larger degree nodes within the highly connected core. Hubs grow through larger degree nodes loosing connections and

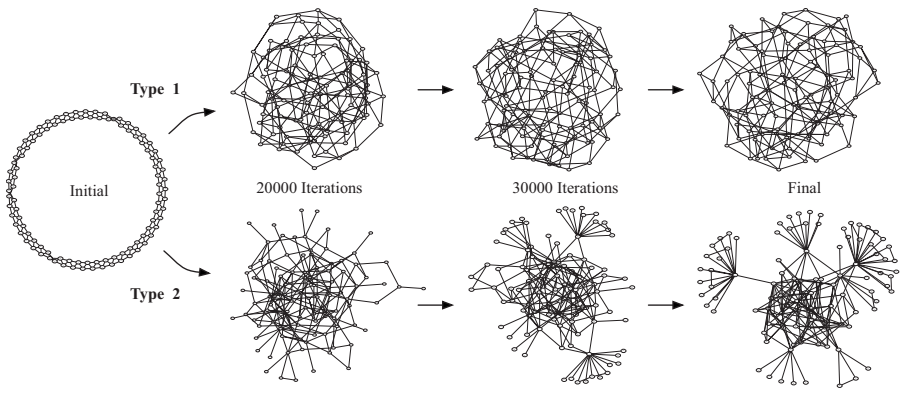

FIG. 7. Alternative stable topologies seen when evolving networks to optimize the order-parameter performance measure with fixed coupling strength $\hat{\sigma}=0.7$.

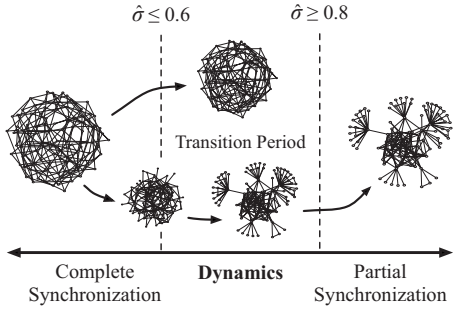

FIG. 9. Topological bifurcation seen when varying the fixed coupling strength $\hat{\sigma}$ used by the order-parameter performance measure during network evolution. The change is driven by factors influencing the underlying realizable dynamics that can be exhibited at a particular coupling strength.

shrink by single degree nodes being reincorporated into the highly connected core. Due to the probability of picking each type being related to their overall number and degree, an equilibrium point will exist where these probabilities become equal with single-degree nodes being added and removed at the same rate. Variation in this value will be due to the stochastic element of the evolutionary process.

B. Topological bifurcation

Transitions between different types of network topology have been extensively studied with regard to generative network models [38]. The most famous of these is found in random graph theory where varying connection probabilities of a standard Erdös-Rényi model lead to a transition from multiple disconnected subgraphs to a single giant connected component [39]. Less work has viewed such transitions from an optimization stand point. This is especially true when considering performance measures based on system-level dynamics, which in turn are intrinsically linked to an underlying network topology. Links can also be made with dynamical systems theory and bifurcation analysis [40]. Unlike a standard bifurcation, where varying a model parameter leads to a qualitatively different system-level behavior, we instead have the situation that varying a model parameter (fixed coupling strength for evolution $\hat{\sigma}$) not only causes a transition in system-level dynamics, but also a significant difference in the final underlying system structure. Due to these similarities, we will refer to such transitions as *topological bifurcations*.

Figure 9 shows a schematic of the topological bifurcation seen in our system. All variables related to dynamics are fixed, apart from the coupling strength $\hat{\sigma}$ used during evolution. This acts as a bifurcation parameter and as it changes, we alter the *realizable* dynamics of the system and so too the topologies providing enhanced synchronization.

Due to dynamical performance measures relying on simulated output from the system, it is difficult to know if the topological bifurcation is intrinsically linked to the Rössler dynamics or if it is a more general feature exhibited by all systems having a master stability function with a bounded stable region. To assess this possibility, additional network evolutions were performed for similar class Γ_2 systems, having Lorenz and Chua node dynamics taken from [33] and a fixed coupling strength $\hat{\sigma}$ larger than the upper bound of the stable region. This places the systems into a regime where type 2 topologies arise for our Rössler dynamics and we would expect similar features to emerge if the structure is independent of node dynamic. These newly evolved networks displayed qualitatively the same type 2 features, with a highly interconnected central region surrounded by hubs connected to lower degree nodes and lend support to the idea that such topologies may hold more generally across other forms of node dynamic when transitioning out of a stable synchronized region.

V. FURTHER FEATURES OF THE EMERGING TOPOLOGIES

To gain a further understanding of the subtle connection structures that may be present in the evolved networks, we employed two further tools often used in the literature on complex networks: *motif analysis* and *B matrices*.

A. Topological motifs

The presence of motifs has been indicated in the literature as a significant feature of many technological and natural networks. It has been suggested that such motifs are bound to appear in evolutionary networks when the network objectives have shared subgoals and are dynamically switched (see [24] and references therein). We test here the presence of motifs in the emerging topologies obtained when considering their synchronization performance. Motif detection was performed using the FANMOD algorithm [41] and limited to motifs of sizes 3 and 4. Each resultant topology was analyzed in comparison to 1000 separately randomized versions of the initial network. Using both the original and these randomized versions, z scores and p values could be calculated for all motifs discovered in the original network. Motif distributions for each type of evolved network are shown in Table III, splitting into three main types.

First, eigenratio-evolved networks display overexpression of motif 5 and underexpression of motifs 3 and 7. These networks also do not contain any motifs of types 6 and 8 due to the low expression of triangles in general equal to 0.1%.

Order-parameter-evolved networks using $\hat{\sigma} \in [0.1, 0.7]$ (type 1) fall into the next category, containing a significantly increased number of triangles at the cost of motif 1. In terms of 4 node motifs, there was overexpression of motifs 4 and 6 in all networks. A few networks with $\hat{\sigma}=0.1$ and 0.6 displayed motif 8 at a very low frequency of 0.011% and 0.002%. However, in relation to our randomized sample, this constituted statistically significant overexpression. Similar to the eigenratio networks, motifs 4 and 7 were also underexpressed although at levels higher than that for eigenratio networks. An interesting feature of these results is the convergence toward the eigenratio distribution as the fixed coupling strength is increased. This trend, however, was only present for the underexpressed motifs.

Evolved networks with $\hat{\sigma}=0.7$ (type 2) have similar features to the previous distribution, but with three main differ-

TABLE III. Average motif frequency for the evolved topologies. Arrows represent statistically significant over ↑ and under ↓ expression of a motif in comparison to a randomized network (p value <0.01).

Evolved topology	1	2	3	4	5	6	7	8
Eigenratio	99.90	0.10	19.71↓	0.20	80.05↑		0.04↓	
Order parameter $\hat{\sigma}$=0.1	97.98↓	2.02↑	24.21↓	3.36↑	71.64	0.10↑	0.67↓	0.011↑
Order parameter $\hat{\sigma}$=0.2	99.25↓	0.75↑	24.33↓	1.63↑	73.48	0.01↑	0.54↓	
Order parameter $\hat{\sigma}$=0.3	99.08↓	0.92↑	24.85↓	2.10↑	72.44	0.03↑	0.57↓	
Order parameter $\hat{\sigma}$=0.4	99.40↓	0.60↑	24.01↓	1.26↑	74.22	0.01↑	0.49↓	
Order parameter $\hat{\sigma}$=0.5	99.02↓	0.98↑	21.48↓	1.95↑	76.09	0.03↑	0.45↓	
Order parameter $\hat{\sigma}$=0.6	96.74↓	3.26↑	15.95↓	5.83↑	77.77↓	0.17↑	0.28↓	0.002↑
Order parameter $\hat{\sigma}$=0.7 (type 1)	97.35↓	2.65↑	17.35↓	4.68↑	77.52↓	0.11↑	0.34↓	
Order parameter $\hat{\sigma}$=0.7 (type 2)	95.83↓	4.17↑	42.36↑	8.82↑	47.07↓	0.42↑	1.31↓	0.010↑

ences. Motifs 3 and 4 are significantly overexpressed attaining values nearly twice that seen before and motif 5 is significantly underexpressed at 47%, in comparison to 70%–80% for all other networks. These characteristics tie in with features seen in Fig. 4(f) but also highlight that development of the fanlike hubs takes place primarily at the expense of motif 5.

In addition to these specific distributions, a more remarkable difference is found when comparing networks evolved using the static eigenratio measure and those obtained through dynamical simulation with the order parameter. If we focus on networks evolved using simulated dynamics (order parameter) *feedback motifs* 2, 4, and 6, associated with closed-loop behavior between node triplets, are found in significantly larger numbers while *branching motifs* 1 and 3 are underexpressed. No such correlation is present for networks evolved using the static eigenratio measure. We conjecture that this feature is due to the fact that when dynamics are explicitly taken into account, the coordination of motion between agents in the network requires local feedback loops to be formed to create stable subregions. These would allow subsets of nodes to shield themselves from perturbations induced by other externally connected nodes. On the contrary, when static measures such as the eigenratio are used, such localized feedback is not required as the "negotiation" between neighboring agents becomes less important. This is due to increased knowledge of favorable *global* features, intrinsically present within the performance measure. Having this additional information results in localized stability being unnecessary for intermediate configurations surrounding optimal states.

This finding may cast light on some of our previous results. In Sec. III D, an increased lower bound of coupling strength for networks evolved using the order parameter was found. It has previously been shown that network girth is maximized for highly synchronizable networks [6]; something illustrated when using the eigenratio performance measure, with our results showing an average girth equal to 3.75. Once this value becomes larger than 3, the evolved topologies will begin to see a complete lack of triangular feedback motifs. From a dynamical perspective, these are required for localized stability. Therefore, it is natural to conclude that when optimizing using the order parameter, intermediate topologies near these optimal states will become unlikely with the process remaining in stable local optima.

In addition, overexpression of similar motifs has been highlighted in the literature for both natural (gene regulation, neural networks, and food webs) and technological networks (electronic circuits and the world wide web) [22].

B. *B* matrices

To compare more subtle properties of the evolved topologies, we made use of the *B matrix*, or *network portrait* as it is also known, introduced by Bagrow *et al.* [42]. This provides a method to visualize and rigorously compare structural information and is defined as the matrix $B=\{b_{lk}\}$, where b_{lk} is the number of nodes that have k members in their respective l shells. An l shell of a given node v_i is defined as the set of nodes at distance l edges away and can be calculated using a breath-first search (BFS) algorithm. The B matrix can be used to view features such as homogeneity and assortativity, in addition to providing a metric to quantitatively calculate distances between topologies.

1. Example: Periodic ring

As an example of how a portrait is created and how some of the visual features translate, we consider the case of an undirected periodic ring. Representative portraits are shown in Figs. 10(a) and 10(b) for even and odd numbers of nodes, respectively.

If we choose any individual node, propagation of the BFS algorithm will lead to the discovery of two new nodes in

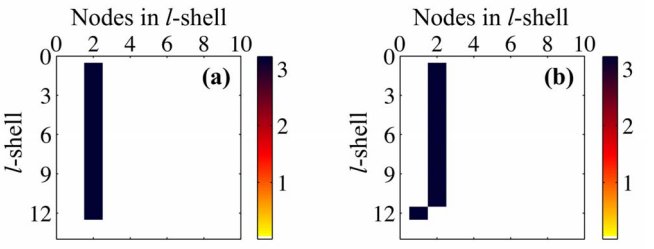

FIG. 10. (Color online) B matrix portraits for (a) 24 and (b) 25 nodes connected in a periodic ring.

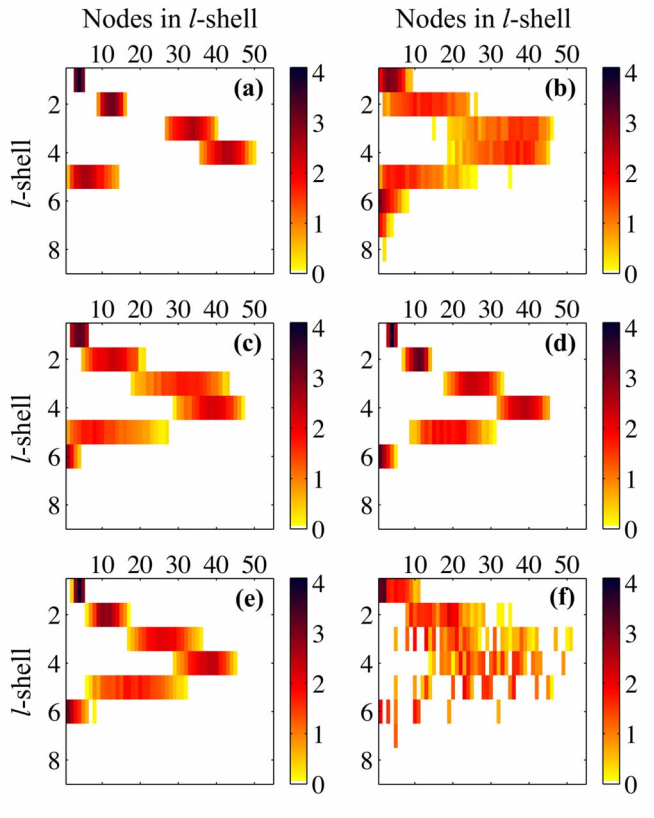

FIG. 11. (Color online) Average B matrix portraits for a selection of performance measures and coupling strengths: (a) eigenratio, order parameter $\hat{\sigma}$=(b) 0.1, (c) 0.5, (d) 0.6, (e) 0.7 (type 1), (f) 0.7 (type 2). Colors represent the number of nodes at a given index within the B matrix and are plotted on a log scale $[\log(b_{lk})]$.

each l shell until a distance of $\lfloor N/2 \rfloor$ is reached. At this point, both directions of propagation around the ring meet; if the number of nodes in the network is even, then the final l shell will only contain a single node, otherwise it will contain two. With all nodes effectively the same due to full rotational symmetry, the contribution of each node to the final portrait will be identical. Specifically, the portrait will contain a value of N at column 2 for rows 1 to $(\lfloor N/2 \rfloor - 1)$ with the value N in column 1 or 2 at row $\lfloor N/2 \rfloor$, depending if N is even or odd.

This example also allows us to link features of the portrait and network topology. First, the high homogeneity is manifested in terms of narrow bands of width 1 at every possible distance. If we had instead considered a case with small variation in node degrees, we would see a widening of all bands as these features were encountered. Bandwidth is therefore heavily related to network homogeneity. Second, because the BFS algorithm finds the shortest path between any two nodes, the maximum row number containing an entry relates to the diameter of the network, $\lfloor N/2 \rfloor$ in this case.

2. Evolved topologies

Figure 11 shows averaged B matrix portraits for several of the evolved network topologies presented in Sec. III. There are three main types of portrait. The first, displayed by the eigenratio-evolved topologies and shown in Fig. 11(a), is characterized by narrow bands separated by large gaps. This translates into a highly homogeneous network with most of the nodes being covered within the first three shells of the network. This is highlighted by the central values of the first four rows leading to an average discovery of 4+12+34 +43=93% of the network. The smaller overall diameter of these networks is also revealed by the last band falling in the fifth row of the matrix, matching the calculated value of 5.25.

Networks evolved using the order parameter for $\hat{\sigma} \in [0.1, 0.7]$ (type 1) fall into the next category and can be seen in Figs. 11(b)–11(e). These share many similarities in their shape to the previous type, however, bands are much wider and the rate at which the network reaches the maximum sized l shell is lower. For example, if we take the $\hat{\sigma}$ =0.6 portrait, the first four rows in this case lead to an average network discovery of 4+11+25+40=80%. An interesting characteristic of this type of network is the convergence toward similar features seen in eigenratio-evolved networks. As the fixed coupling strength $\hat{\sigma}$ is increased, band widths narrow, gaps begin to form, and the diameter is reduced.

Finally, $\hat{\sigma}$=0.7 (type 2) networks displayed a very fine structure with multiple separated bands at most distances [see Fig. 11(f)]. The hubs present in the topology that are connected to many single degree nodes are linked to the six narrow bands seen in the sixth row of the portrait.

We also analyzed how a single evolution looks in terms of the associated B matrix. Figure 12 shows the evolution of a $\hat{\sigma}$=0.6 network with the B matrix plotted at points throughout the process. The initial topology of a regular one-dimensional lattice is immediately visible in (a) by the single

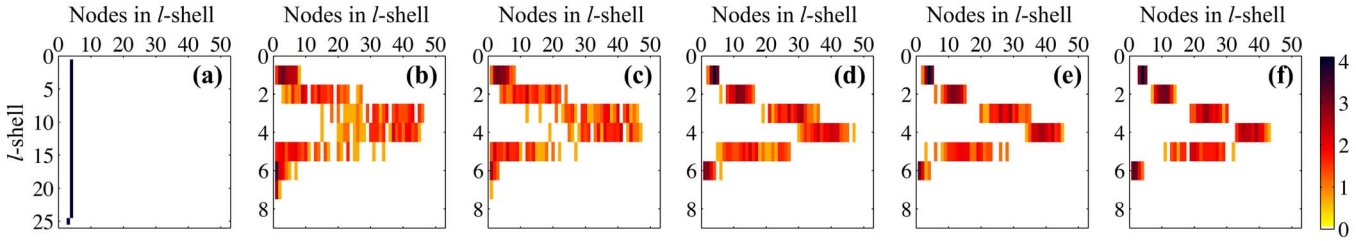

FIG. 12. (Color online) Evolution of a B matrix portrait when using the order-parameter performance measure with $\hat{\sigma}$=0.6. Initial topology was a periodic ring lattice with nearest and next-nearest-neighbor coupling. B matrices were taken at iterations (a) 1, (b) 4000, (c) 8000, (d) 14 000, (e) 20 000, and (f) 180 000. Colors represent the number of nodes at a given index within the B matrix and are plotted on a log scale $[\log(b_{lk})]$.

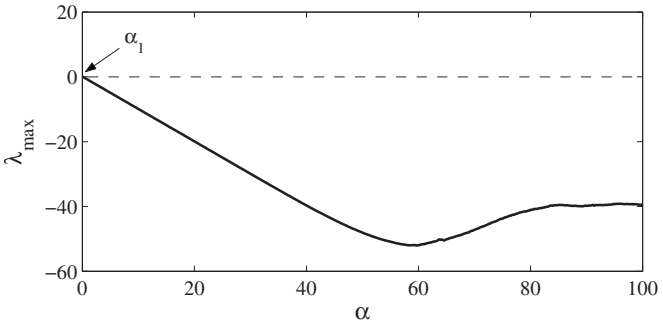

FIG. 13. Master stability function for the chosen Rössler system coupled on all internal states with $\alpha_1 \approx 0.0831$.

narrow band, but what is interesting is the speed at which this structure is lost. After 4000 iterations, it is impossible to see any of the original latticelike structure. This randomization is partly due to the method of evolution which accepts many configurations that are not improvements when the temperature is high. Another characteristic shown at this stage is the reduction in graph diameter, with the extent of portrait in terms of rows falling from 25 to just 7. As the evolution progresses, we now see a reduction in fine grain structure with a move toward continuous bands relating to increased homogeneity at varying distances. The final change is a narrowing of bands, leading to gaps across rows. This feature helps to reduce the variance in possible rates of network exploration due to a similar number of nodes being discovered as distance increases. In summary, evolution toward a final topology produces two main types of feature: lowered network diameter and increased homogeneity.

VI. BOUNDED SYNCHRONIZATION

The assumption of identical node dynamics breaks for the majority of real-world systems. Variability is naturally present due to the physical uniqueness of components and differences in local environmental conditions.

In this section, we attempt to isolate how variability of individual oscillator dynamics impacts system-level synchronization and investigate the features that arise when an alternative dynamical performance measure is used. We consider a similar system to that in Sec. III, however, simplify it so as to isolate the impact node variability has on the evolved topologies. First, we alter the internal node coupling to occur on all oscillator states, changing the master stability function to a class Γ_1 type [33] (see Fig. 13). The new system has a stable region in the range $\alpha \in (0.0831, +\infty)$ with no upper bound on the coupling strengths able to achieve full synchronization. This has the benefit of removing the desynchronizing bifurcation seen for $\sigma > 0.7$, reducing the influencing factors on our results. Furthermore, a large fixed coupling strength $\hat{\sigma}=1$ was selected to ensure full synchronization is possible when all oscillator dynamics are identical. Heterogeneity of individual oscillators is introduced by uniformly at random perturbing each nodes parameters by a set amount (1%, 5%, 10%, 25%, and 50%).

Due to no common solution existing between all oscillators, it is necessary to introduce a new measure of synchronization. Using a similar approach to [43], we consider the size of the bounded set of trajectories as $t \to \infty$. This provides an indication of how closely the trajectories come to some average solution and was used as the basis of the *bounded synchronization measure* $\phi \in \mathbb{R}^+$ calculated as follows:

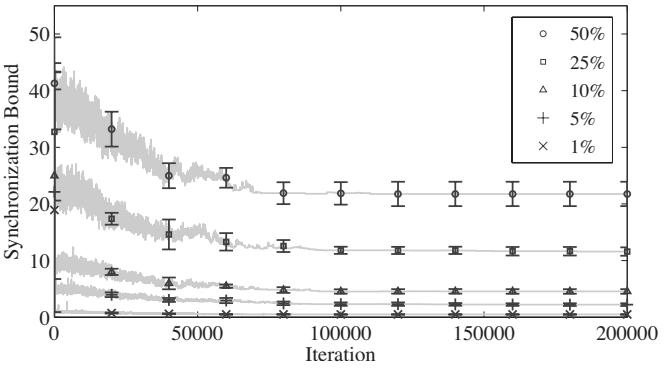

FIG. 14. Change in bounded synchronization during the evolution of networks with differing variation in underlying model parameters (1%–50%).

$$\phi(t_1,t_2) = \max\{d_{ij}(t) | i,j \in N,\ t_1 \le t \le t_2\}. \tag{5}$$

Here, N is the number of nodes in the network equal to 100, t_1 is a time chosen after the settling time, t_2 is the final simulation time (necessary to understand variation among trajectories), with $t_2 > t_1$, and $d_{ij}(t)$ is the standard Euclidean norm distance between the trajectories of nodes i and j at time t. After simulation with a range of parameter values, we selected $t_1=150$ and $t_2=200$ in order to capture the required dynamic characteristics.

Using this performance measure, networks were evolved to minimize the overall bound. Results are presented in Table IV illustrating that even with large parameter variability, topology can have a dramatic effect in significantly reducing the final bound. Greatest improvement is seen for smaller parameter variation, however, large improvements of 47.3% are seen even at 50% parameter variation. In addition, standard deviation of the final bound is positively correlated with the parameter variation (see Fig. 14).

To allow for comparison to results in previous sections, standard statistical analysis was performed and B matrices and motifs were calculated. These all showed similar features to previous networks evolved using the order-parameter

TABLE IV. Comparison of synchronization bounds with variability related to the percentage change applied uniformly at random to each of the oscillator parameters.

Variability	Initial ϕ	Final ϕ	$\pm$%
50%	41.3	21.8	−47.3
25%	32.7	11.6	−64.6
10%	25.0	4.6	−81.8
5%	22.1	2.2	−90.0
1%	18.9	0.5	−97.5

TABLE V. Average motif frequency for networks evolved to minimize the bounded synchronization measure for differing amounts of model parameter variation. Arrows represent statistically significant over ↑ and under ↓ expressions of a motif in comparison to a randomized network (p value <0.01).

Parameter variation	 1	 2	 3	 4	 5	 6	 7
1%	98.82↓	1.17↑	22.84↓	2.35↑	74.23 –	0.06↑	0.54↓
5%	98.81↓	1.19↑	24.39↓	2.43↑	72.35 –	0.06↑	0.79↓
10%	98.50↓	1.50↑	24.32↓	3.14↑	71.84 –	0.13↑	0.63↓
25%	98.50↓	1.50↑	24.35↓	3.32↑	71.51 –	0.11↑	0.72↓
50%	99.06↓	0.94↑	23.63↓	1.92↑	73.72 –	0.05↑	0.70↓

measure for $\hat{\sigma} \in [0.3, 0.6]$, with reduced diameter, and narrow degree and betweenness distributions. B matrices also showed no significant differences in the structural features between these topologies.

In contrast, the average motif distributions displayed in Table V did reveal some surprising results. Overall, each network showed a statistically significant overexpression of local feedback motifs 2, 4, and 6 supporting the idea presented in the previous section that stabilizing features are important for evolutionary processes that are intrinsically linked to the dynamical performance. Furthermore, the amount of this feedback grows with parameter variation up to 25%, with increases of 28%, 41%, and 83% for motifs 2, 4, and 6, respectively. This is also logical if such feedback is being used for stability as larger variation in dynamics will require increased control effort.

As parameter variation is increased further to 50%, a very different behavior is seen. At this point, although feedback motifs are still statistically overexpressed, large drops occur in overall frequency. We see decreases of 37%, 42%, and 55% for motifs 2, 4, and 6 in comparison to results at 25% parameter variation. A possible explanation for this unusual behavior links to the divide in influence that node and edge dynamics have over network topology in relation to the overall system-level dynamic. As stated previously, it is known for networks of identical oscillators that topology has a major effect on the overall synchronizability. However, as the dynamics of individual nodes significantly diverge, the impact of topology becomes reduced. This implies the existence of a threshold at which, altering network topology would have little effect and may be the cause for the drop in feedback seen in our results. At this point, increasing the number of feedback motifs would have little effect and so as expected would be seen less in our evolved topologies.

VII. CONCLUSION

We have shown that synchronization can be enhanced by considering the simulated output of a dynamical network during evolution of the topology. Starting with a homogeneous network of identical oscillators for $\hat{\sigma} \in [0.3, 0.6]$, evolving networks using the order-parameter performance measure showed an improvement in the fraction of nodes synchronized over a range of simulated coupling strengths, roughly centered around the fixed coupling strength used during evolution. Final topologies displayed a convergence toward our control networks that were evolved using the eigenratio, a common measure of synchronizability. Features included reduced diameter and narrow degree and betweenness distributions.

The presence of a topological bifurcation and bistability was found as the topology transitioned toward an enhanced form for $\hat{\sigma} \geq 0.8$. These networks showed very different characteristics with reduced homogeneity through the formation of hubs on the exterior of a central highly connected component. Although B matrix analysis confirmed significant differences between these final structures, motif distributions of all networks evolved using the dynamical order parameter showed a common statistically significant overexpression of three-node feedback motifs: something not displayed by networks evolved using the topological eigenratio measure. We conjecture that localized feedback loops are vital in evolved networks that use a dynamical measure to help stabilize the behavior exhibited by groups of nodes in the system.

Generality of the topological bifurcation was assessed for several other types of node dynamic and in each case qualitatively similar features were seen. This supports the idea that type 2 topologies may be a more general feature exhibited when a system transitions out of a stable synchronized region, for example, due to an increase in coupling strength. Even so, the effects that other aspects of the system have on the evolved topologies, such as nonlinear coupling between nodes, remain as possible future directions for this work.

These results also illustrated a fundamental difference and tradeoff made between topological (eigenratio) and dynamical (order parameter) measures. Topological measures can robustly generate high-performance structures, but are limited to understood areas of the system dynamic. For example, one can only improve synchronization when the system is placed within the stable region of the master stability function. In contrast, dynamical measures while improving a systems performance, although to a lesser extent than the topological measures, can also adapt. This allows for the generation of different types of topology as factors influencing the systems performance change. Furthermore, they pose no constraints on the form of the system, providing improved topologies for a much broader range of scenario and including those where topological measures have yet to be found. Finally, we showed that when considering heterogeneous networks of nonidentical oscillators, bounded synchronization can be used as a performance mea-

sure to reduce the maximum distance between trajectories as $t \to \infty$.

While localized feedback is prevalent in the evolved networks, the question of how such motifs combine to improve synchronization over larger scales remains unanswered. This is vital if practical use is to be made of our findings and will be pursued in future work. Further investigation will also be required to determine the generality of such feedback for differing models of node dynamic and whether such features are displayed in directed networks and evolved systems that exhibit synchronization.

ACKNOWLEDGMENTS

We would like to thank Professor Erik Bollt and Dr. Jim Bagrow for their helpful discussions on network analysis and the calculation of B matrices. Also, we are grateful to the anonymous reviewers for their useful comments. T.E.G. acknowledges the support of EPSRC-GB Grant No. EP/5011214. All simulations were carried out using the computational facilities of the Advanced Computing Research Centre, University of Bristol—http://www.bris.ac.uk/acrc/.

[1] S. Boccaletti, V. Latora, Y. Moreno, M. Chavez, and D. Hwang, Phys. Rep. **424**, 175 (2006).
[2] D. Bell-Pedersen, V. Cassone, D. Earnest, S. Golden, P. Hardin, T. Thomas, and M. Zoran, Nat. Rev. Genet. **6**, 544 (2005).
[3] L. Glass, Nature (London) **410**, 277 (2001).
[4] L. M. Pecora, T. L. Carroll, G. Johnson, and D. Mar, Phys. Rev. E **56**, 5090 (1997).
[5] L. M. Pecora and T. L. Carroll, Phys. Rev. Lett. **80**, 2109 (1998).
[6] L. Donetti, P. I. Hurtado, and M. A. Muñoz, Phys. Rev. Lett. **95**, 188701 (2005).
[7] K. Kaneko, Physica D **41**, 137 (1990).
[8] S. C. Manrubia and A. S. Mikhailov, Phys. Rev. E **60**, 1579 (1999).
[9] M. G. Rosenblum, A. S. Pikovsky, and J. Kurths, Phys. Rev. Lett. **76**, 1804 (1996).
[10] L. M. Pecora, Phys. Rev. E **58**, 347 (1998).
[11] A. Rad, M. Jalili, and M. Hasler, Chaos **18**, 037104 (2008).
[12] S. Boyd, Proceedings of the International Congress of Mathematics, 2006, Vol. 3, p. 1311 (unpublished).
[13] S. Yook and H. Meyer-Ortmanns, Physica A **371**, 781 (2006).
[14] L. Donetti, F. Neri, and M. Muñoz, J. Stat. Mech.: Theory Exp. 2006, P08007.
[15] M. Parter, N. Kashtan, and U. Alon, PLOS Comput. Biol. **4**, e1000206 (2008).
[16] P. Oikonomou and P. Cluzel, Nat. Phys. **2**, 532 (2006).
[17] H. Qin, H. Lu, W. Wu, and W. Li, Proc. Natl. Acad. Sci. U.S.A. **100**, 12820 (2003).
[18] P. François and V. Hakim, Proc. Natl. Acad. Sci. U.S.A. **101**, 580 (2004).
[19] J. Mason, P. Linsay, J. Collins, and L. Glass, Chaos **14**, 707 (2004).
[20] S. Paladugu, V. Chickarmane, A. Deckard, J. Frumkin, M. McCormack, and H. Sauro, IEE Proc.-Syst. Biol. **153**, 223 (2006).
[21] K. Kaneko, Chaos **18**, 026112 (2008).
[22] R. Milo, S. Shen-Orr, S. Itzkovitz, N. Kashtan, D. Chklovskii, and U. Alon, Science **298**, 824 (2002).
[23] U. Alon, Nat. Rev. Genet. **8**, 450 (2007).
[24] N. Kashtan and U. Alon, Proc. Natl. Acad. Sci. U.S.A. **102**, 13773 (2005).
[25] S. Mangan and U. Alon, Proc. Natl. Acad. Sci. U.S.A. **100**, 11980 (2003).
[26] J. Tyson, K. Chen, and B. Novak, Curr. Opin. Cell Biol. **15**, 221 (2003).
[27] N. Kashtan, S. Itzkovitz, R. Milo, and U. Alon, Phys. Rev. E **70**, 031909 (2004).
[28] I. Lodato, S. Boccaletti, and V. Latora, EPL **78**, 28001 (2007).
[29] T. E. Gorochowski, M. di Bernardo, and C. S. Grierson (unpublished).
[30] J. Dreo, A. Petrowski, P. Siarry, and E. Taillard, *Metaheuristics for Hard Optimization* (Springer, New York, 2005.
[31] G. Csárdi and T. Nepusz, InterJournal Complex Systems 1695 (2006), http://igraph.sf.net
[32] M. Galassi, J. Davies, J. Theiler, B. Gough, G. Jungman, M. Booth, and F. Rossi, *GNU scientific library* (2002).
[33] L. Huang, Q. Chen, Y. C. Lai, and L. M. Pecora, Phys. Rev. E **80**, 036204 (2009).
[34] A. Wolf, J. Swift, H. Swinney, and J. Vastano, Physica D **16**, 285 (1985).
[35] M. Newman, A. L. Barabási, and D. J. Watts, *The Structure and Dynamics of Networks* (Princeton University Press, Princeton, 2006.
[36] S. Fallat and S. Kirkland, Electron. J. Linear Algebra **3**, 48 (1998).
[37] A. E. Motter, C. Zhou, and J. Kurths, Phys. Rev. E **71**, 016116 (2005).
[38] I. Derényi, I. Farkas, G. Palla, and T. Vicsek, Physica A **334**, 583 (2004).
[39] P. Erdös and A. Rényi, Publ. Math. (Debrecen) **6**, 290 (1959).
[40] U. A. Kuznetsov, *Elements of Applied Bifurcation Theory* (Springer, New York, 1998).
[41] S. Wernicke and F. Rasche, Bioinformatics **22**, 1152 (2006).
[42] J. Bagrow, E. Bollt, J. Skufca, and D. Ben-Avraham, EPL **81**, 68004 (2008).
[43] D. J. Hill and J. Zhao, CDC 2008, 47th IEEE Conference on Decision and Control, 817 (2008).